Study on the Thickness Effect of 3PB Specimen on Dimple Fracture Processes.

Masanori Kikuchi[1]

SUMMARY

Three-Point-Bend (3PB) specimens with different thickness are used for fracture toughness test. By the SEM (Scanning Electron Microscope) observation, it is shown that the roughness of fracture surface is different from each other largely. They are the effect of constraint condition. The dimple fracture process is simulated by the finite element method using Gurson's constitutive equation, and the crack tip stress fields are obtained. The distributions of stress triaxiality components are qualitatively agree with the experimental results. The J-R curves obtained also qualitatively agree with those of experiments, and the fracture surface roughness is well simulated.

INTRODUCTION

It has been shown experimentally that the apparent fracture toughness is largely affected by the condition of constraint at the crack tip. It is called constraint effect and has been studied by Anderson[1], Sorem *et al*.[2] and O'Dowd *et al*.[3]. From the practical viewpoint, this effect is evaluated by the local approach. The change of the apparent fracture toughness is well estimated using this approach by Xia *et al*.[4], Ruggieri *et al*.[5] and Koers *et al*.[6]. But the effect of the constraint on the microscopic fracture process has not been studied yet. In this series study, the effect of loading condition and that of initial crack length have been studied [7]. In this paper, the effect of the specimen thickness of 3PB specimen on the fracture process is studies in detail. The fracture surface is observed using SEM after fracture test. The FEM analysis is conducted using Gurson's constitutive equation and the dimple fracture process is simulated. The effect of the change of the constraint condition at the crack tip on the dimple fracture process is studied and discussed.

EXPERIMENT

Figure 1 shows the shape and size of Three-Point-Bend (3PB) specimen used in this study. The thickness of 3PB specimen, B, is changed in three cases, 8mm, 4mm and 2mm. The material of the specimen is A533B steel, which is used for the reactor pressure vessel. By the fracture toughness testing standard [8], the thickness of this specimen should be larger than 7mm. B=8mm specimen satisfies this condition, though B=4mm and 2mm specimens don't satisfy it. By comparing three specimens, the effect of constraint along thickness direction is understood well.

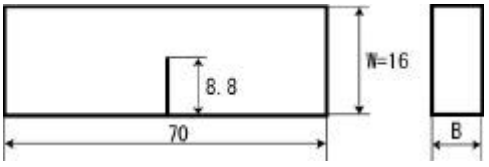

Figure 1: Configuration of 3 kinds of specimen.

Fig.2 shows the crack tip stress field obtained by three-dimensional FEM analyses based on J2 flow theory. These data are obtained at the mid-plane of each specimen. Result of HRR solution

[1] Department of Mechanical Engineering, Tokyo University of Science, 2641, Yamazaki, Noda, Chiba, 278-8510, Japan

[9] is also plotted in this figure. It is shown that the stress field of B=8mm specimen agrees with HRR solution well. It means that the crack tip stress field is in plane strain condition and the crack tip is under strong constraint. As the thickness becomes thinner, B=4mm and 2mm, the crack tip stress field deviates from HRR solution gradually. It means that the constraint becomes weak with the decrease of the specimen thickness.

Using these specimens, fracture toughness values are obtained. Figure 3 shows J-R curves obtained by the fracture toughness test. It is noticed that R-value of thick specimen during stable crack growth is larger than that of thin specimen. By this figure, J_{IC} values are obtained for each specimen. The results are shown in Table 1. The J_{IC} value of B=8mm specimen is considered to be a valid J_{IC} value. Results of other two specimens show larger value than the valid one.

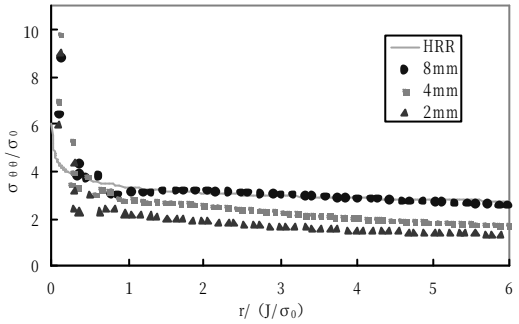

Fig.2 Crack tip stress field at the specimen mid-plane.

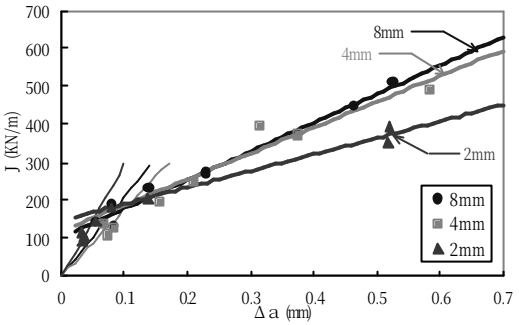

Fig.3 J-R curves by experiments.

Table 1 J_{IC} value of three specimens.

Thickness (mm)	8	4	2
J_{IC} Value (KN/m)	158.0	194.1	171.6

Fracture surfaces are observed using Scanning Electron Microscope, and the dimple diameters are measured. Figs.4(a) and (b) show SEM photos for B=8mm and 2mm specimens. They are photos at the mid-plane of each specimen. It is noticed that large dimples are observed in thick specimen, though they are not observed in thin specimen. In general, the dimple diameter value changes in wide range. Some are larger than 100 μm, and some are under 1 μm. In this study, larger voids, which are considered to be nucleated in the early stage of dimple fracture and have large effect on fracture process, are mainly considered. Number of voids larger than 10 μm is counted for three specimens, and the average diameter of them is shown in Table 2. The average dimple diameter changes with the change of the specimen thickness. Thick specimen results large dimple diameter, and as the thickness decreases, it also decreases.

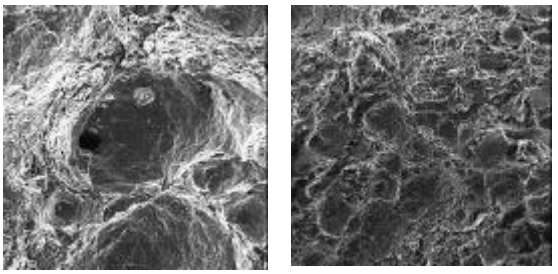

(a) 8mm (b) 2mm

Fig.4 Fracture surface photos of 3PB specimens.

Table 2 Average dimple diameter.

Thickness (mm)	8	4	2
Diameter (μm)	22.2	17.7	17.0

Fig. 5 shows the crack growth patterns for three specimens. In this figure, the abscissa is the position along the crack front. Both sides show specimen surfaces, and the center is the mid-plane of the specimen. The ordinate is the crack growth amount. In 8mm thick specimen, the crack growth occurs in wide area along the crack front. But in 2mm thick specimen, crack growth occurs mainly at the mid-part of the specimen. As a result, the crack front configuration becomes steep in thin specimen. In 2mm thick specimen, the fracture mode at specimen surface is shear type fracture, and shear-lip is observed.

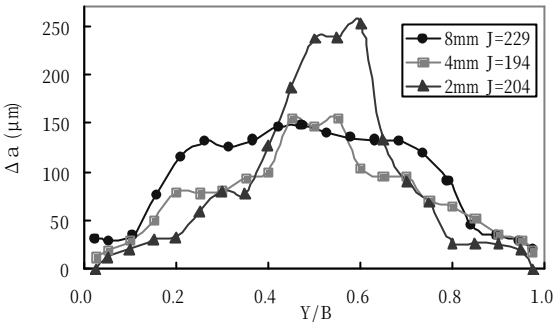

Fig.5 Crack growth amount along the crack front.

FEM ANALYSIS

1. Gurson's constitutive equition

To consider the microscopic fracture process, the simulation of the nucleation, growth and coalescence of voids is needed. For this purpose, FEM analysis using constitutive equation proposed by Gurson and later modified by Tvergaard is conducted [10]. This constitutive equation is shown as follows.

$$\Phi = \frac{3}{2}\frac{s'_{ij}s'_{ij}}{\overline{s}_m^2} + 2f^* q_1 \cosh\left(\frac{q_2 s_{kk}}{2\overline{s}_m}\right) - \left(1 + q_1^2 f^{*2}\right) \tag{1}$$

where s'_{ij} is the deviatric stress, $\overline{s}_m$ is the equivalent stress, f^* is the void volume fraction and q_1, q_2 are constants proposed by Tvergaard. The rate of increase of void volume fraction is shown as follows.

$$\dot{f} = (1-f)\dot{e}^p_{kk} + A(\dot{\overline{s}}_m + \dot{s}_{kk}/3) + B\dot{\overline{e}}^p_m \tag{2}$$

The first term in equation (2) accounts for the growth of existing voids, the second term models the nucleation of voids by a stress controlled mechanism, while the third term corresponds to plastic strain controlled void nucleation. In this paper, plastic strain controlled nucleation is considered, and parameters A and B are given as follows.

$$A = 0,\ B = \frac{f_N}{S_N\sqrt{2p}}\exp\left[-\frac{1}{2}\left(\frac{\overline{e}^p - e_N}{S_N}\right)^2\right] \tag{3}$$

where f_N is volume fraction of void nucleating particles, S_N is the corresponding standard deviation, e_N is the mean strain for nucleation.For the use of Gurson's model, the finite deformation analysis is needed.

2. Numerical model

It is well known that the results by Gurson's model depend largely on the mesh size. By this reason, the comparison of the numerical results with those by experiment is meaningless. In the

following analyses, same mesh size is employed at the crack tip for all models. Results are compared with those by experiment qualitatively, not quantitatively. The comparative changes of the results with the change of the specimen thickness are studied and discussed.

Fig.6(a) shows the mesh pattern of the 8mm thick specimen. Fig.6(b) is a mesh pattern around the crack front. As the pre-crack introduced by fatigue has some curvature, the crack front is modeled by measuring the real crack front configuration experimentally. The total number of element and number of node for each model is shown in Table 3. As large number of nodes is used in modeling, single CPU is not enough to solve this problem. Parallel computing is employed, and 8 PC Cluster is used.

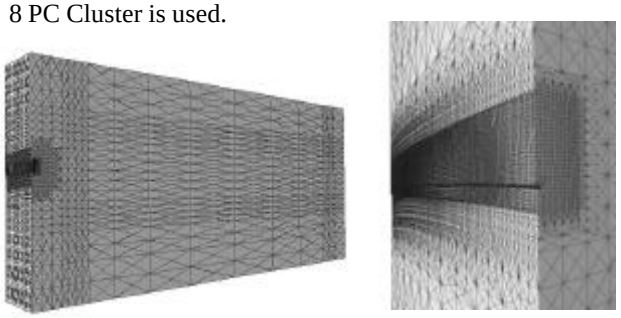

(a) Full mesh (b) Crack front area.
Fig.6 Mesh pattern of 8mm thick specimen.

Table 3 Mesh size.

	Nodes	Elements
8mm	474028	92900
4mm	247298	48230
2mm	134568	26020

3. Numerical results

Fig.7 shows the distributions of stress triaxiality around the crack tip for three specimens. These are just after the dimple fracture initiation at the mid-plane of the specimen. As the thickness decreases, high stress triaxiality area decreases. The highest value also decreases with it. It is also noticed that high stress triaxiality area is wide along thickness direction in thick specimen, and it becomes narrow as thickness decreases. Stress triaxiality affects largely on the nucleation and growth of void, which plays main role in dimple fracture. These figures are deeply related with experimental results shown in Fig.4, where large voids are observed in thick specimen and voids become small in thin specimen.

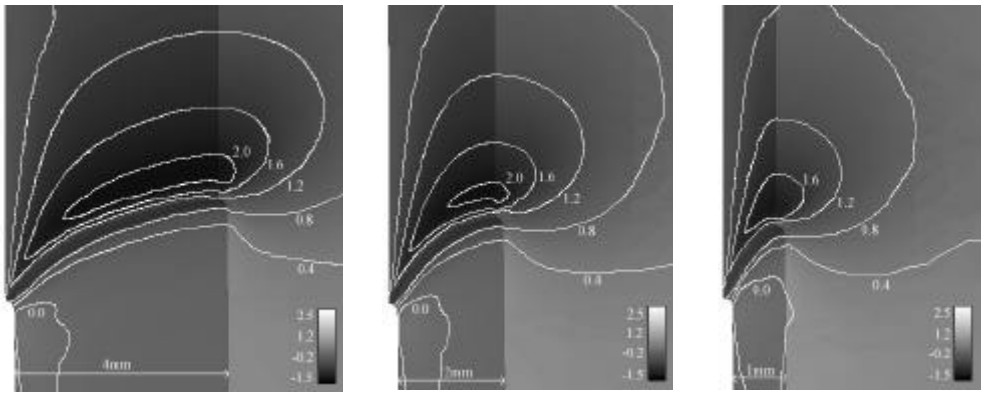

(a) 8mm (b) 4mm (c) 2mm
Fig.7 Stress triaxiality distributions around the crack tip.

Fig.8 shows the distribution of void volume fraction along the crack front for three specimens. Results are similar to those of stress triaxilality distributions. For thick specimen, high void volume fraction area is widely spread in the specimen thickness direction, though it is narrow in thin specimen. It also agrees qualitatively with the experimental results.

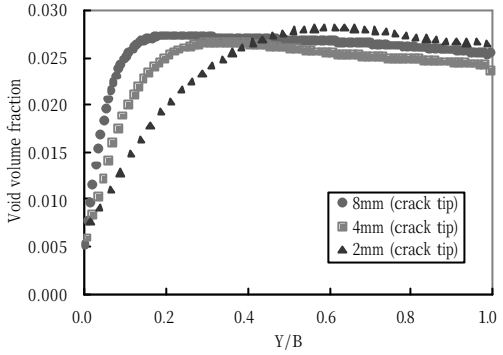

Fig.8 Void volume fraction distribution.

Fig.9 shows crack growth patterns for three specimens. These figures are the results when J value is nearly 200kN/m, after large amount of dimple fracture growth. Results are related with those of Fig.7 and Fig.8. Dimple fracture occurs in wide area in 8mm thick specimen. But in 2mm thick specimen, dimple fracture occurs only at the mid-plane, and steep crack front configuration is generated. In this simulation, shear lip type fracture process is not considered. In the real specimen, shear lip fracture occurs in 2mm thick specimen at both crack edges. But finally, the crack growth amount is the largest at the mid-plane of the specimen, which quantitatively agrees with these numerical simulations.

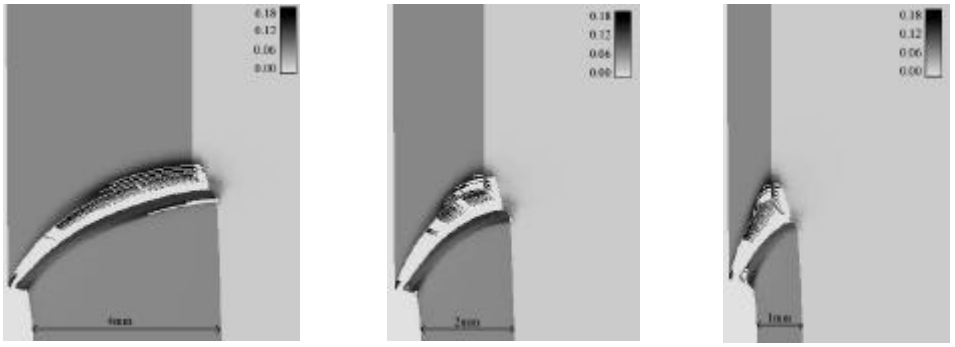

(a) 8mm (b) 4mm (c) 2mm

Fig.9 Crack growth patterns for three specimens.

5 J-R Curves

Fig.10 shows J-R curves obtained by numerical simulation. The ordinate, J integral value, is evaluated using conventional equation using the load-displacement data obtained numerically. The line integration is also conducted. But after some amount of crack growth, plastic zone spreads widely, and J integration path crosses with the plastic zone. Then valid J value is not obtained by line integration. The abscissa is crack growth amount. It is determined as the average at 5 points along the crack front, due to the fracture toughness testing standard [9]. Similar to experimental result, Fig.2, J-R curve of thick specimen is higher than that of thin specimen. In my previous paper [8], the J-R curve becomes high for low-constraint condition, and low J-R curve is obtained

for high constraint condition. In this study, thick specimen is under high constraint condition and thin specimen is under low constraint condition. It is obvious by the numerical results shown in Fig.3. But the results show that high constraint condition specimen results high J-R curve. It is contrary to the previous paper.

The reason of this tendency is due to the method to determine the crack growth amount experimentally. By the fracture toughness standard, the crack growth amount is defined as the average of 5 points along the crack front. These 5 points are near the mid-plane of the specimen. As shown in Fig. 11, the distribution patterns of crack growth amount along crack front are largely different from each other in three specimens. In thick specimen, crack growth amount is nearly constant along the crack front, but it changes largely in thin specimen. By measuring near the mid-plane, the crack growth amount of thin specimen is evaluated largely than that of thick specimen. This is the main reason of the difference of J-R curves due to the difference of the specimen thickness.

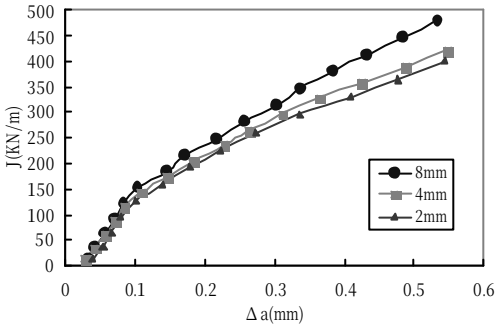

Fig. 10 J-R curves of three specimens.

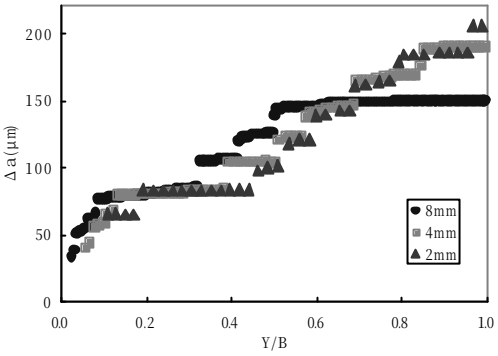

Fig.11 Crack growth amount along crack front.

4. CONCLUDING REMARKS

The thickness effect on the dimple fracture process of 3pb specimen is studied by experiment and numerical simulation. The change of the constraint condition due to the change of the specimen thickness affects on both microscopic and macroscopic dimple fracture process. Numerical simulation agrees well with those experimental phenomena qualitatively.

REFERENCES

1. Anderson. T. L., Int. J. Fracture 41 (1989), p.79-104
2. Sorem. W. A., Dodds. R. H. and Rolfe. S. T., Int. J. Fracture 47 (1991) p.105-126
3. O'Dowd N. P and Shih C. F., J. Mech. Phys. Solids 39 (1991), p.989-1015
4. Xia L. and Shih C. F., J. Mech. Phys. Solids 44 (1996), p.603-639
5. Ruggieri C. and Dodds Jr., Int. J. Fracture 79 (1996), p.309-340
6. Koers R. W. J., Kroom A. H. M. and Bakker A., ASTM STP 2 (1995), p.1244
7. Kikuchi, M., Proc. ICCES03, (2003)
8. JSME Standard S-0001, Japan Society of Mechanical Engineers, (1981)
9. Hutchinson, J.W., J. Mech. Phys. Solids, vol.16 (196), p.13
10. Tvergaard. V., Int. J. Fracture 18 (1982), p.237-252